Sustainable Cities and Society 100 (2024) 104992

Contents lists available at ScienceDirect

Sustainable Cities and Society

journal homepage: www.elsevier.com/locate/scs

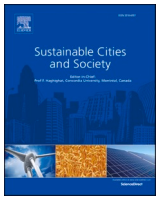

Phosphate activated geopolymer-based coating with high temperature resistance for sub-ambient radiative cooling

Ning Yang [a], Qingdong Xuan [a,b,*], Yang Fu [c], Xue Ma [c], Dangyuan Lei [c], Jianlei Niu [d], Jian-Guo Dai [a,*]

[a] Department of Civil and Environmental Engineering, The Hong Kong Polytechnic University, Hom Hung, Hong Kong, China
[b] Department of Refrigeration and Cryogenics Engineering, Hefei University of Technology, 193 Tunxi Road, Hefei, 230009, China
[c] Department of Materials Science and Engineering, City University of Hong Kong, Kowloon Tong, Hong Kong, China
[d] Department of Building Environment and Energy Engineering, The Hong Kong Polytechnic University, Hom Hung, Hong Kong, China

ARTICLE INFO

Keywords:
Phosphate geopolymer
Coating
Radiative cooling
High temperature resistance
Energy-saving simulation

ABSTRACT

Passive sub-ambient daytime radiative cooling (SDRC) is an energy-free method enabling heat dissipation away from buildings or infrastructures to cold outer space (~3 K). However, although organic coatings (based on polymer matrices) have been proven to be a cost-effective means to achieve the SDRC effect by incorporating various functional fillers, organic coatings may have environmental concerns and aging problems. Herein, an inorganic phosphate activated geopolymer-based (PAGP) SDRC coating was synthesized using nano-silica (SiO_2) particles and barium sulfate ($BaSO_4$) sheets as the modifiers. The synthesized coating could achieve high infrared emissivity of 0.9634 and solar reflectance of 0.9471, which was also found to exhibit high-temperature resistance and optical stability up to 1000 °C due to its covalently bonded structure and electrically neutral system. The chemical composition, surface morphology, and elemental distribution of the coating were characterized by XRD, FTIR, SEM, BET, and EDS. The evolution of condensed structures and weight loss analysis during the high-temperature treatment was conducted by TGA and XRD to analyze the dehydration process and phase change during the heat process. The outdoor field tests showed a maximum sub-ambient temperature reduction of 3.8 °C by the developed coating without any energy input under direct sunlight in Hong Kong. Furthermore, the energy-saving performance of the PAGP-based SDRC coating is analyzed under different climatic conditions in China with the aid of EnergyPlus. Simulation results demonstrated that the PAGP-based SDRC coating can significantly save the cooling load in all five selected cities, which shows great potential in building energy conservation and carbon emission reduction.

1. Introduction

Buildings account for about 40 percent of the world's annual energy consumption, most of which is used to provide electricity-powered air conditioning (Omer, 2008; Pan & Zhang, 2020). The current trend is leading to a severe global warming problem and the intensification of the urban heat island effect, while the misuse of air conditioning has exacerbated environmental degradation by consuming large amounts of energy and emitting greenhouse gasses, which shows significant negative impacts on life quality of people and the sustainable development of cities (Sheng et al., 2023; Younes, Ghali & Ghaddar, 2022). Therefore, continuous efforts have been made to enhance the energy efficiency of buildings and to reduce the energy consumption for cooling, heating and ventilation. In recent years, sub-ambient daytime radiative cooling (SDRC) technology, which can directly dissipate heat to the cold outside space by infrared radiation relying on the transparency of the atmospheric window (8–13 μm) to achieve passive radiative cooling, has attracted increasing attention worldwide (Sun, Wang, Guo, Bao & Bai, 2022; Yuan, Yin, Yuan, Yang & Xu, 2022; Zhai et al., 2017; Zhao, Hu, Ao, Chen & Pei, 2019). The SDRC technology offers an attractive strategy for mitigating global warming by directly dumping heat into outer space without required driving power (Hu et al., 2021; Liu et al., 2023). Since the first validation of the sub-ambient radiative cooling effect in 2014 (Raman, Anoma, Zhu, Rephaeli & Fan, 2014), many kinds of SDRC materials have been developed (Yu, Chan & Chen, 2021), among which, organic coatings (based on polymer matrices) have been proven to be a

* Corresponding authors.
E-mail addresses: qingdongxuan@hfut.edu.cn (Q. Xuan), cejgdai@polyu.edu.hk (J.-G. Dai).

https://doi.org/10.1016/j.scs.2023.104992
Received 26 August 2023; Received in revised form 9 October 2023; Accepted 9 October 2023
Available online 11 October 2023

cost-effective means to achieve the SDRC effect by incorporating various functional fillers (Mandal et al., 2018; Zhai et al., 2017).

However, organic coatings may have environmental concerns because they may release volatile organic compounds (VOCs) into the surrounding environment during the coating formation process. Moreover, the service life of conventional organic coatings is also a concern, as polymeric materials can suffer from aging problems when exposed to UV radiation and elevated temperatures. Long-term outdoor exposure can break the molecular chains of the polymers, resulting in embrittlement of the polymer matrices (i.e., cracking and chalking) and deterioration of the coating-substrate interface (e.g., peeling) (Rong, Wang, Xing & Zhao, 2021; Song et al., 2022). Last but not least, polymer materials are easily combustible. The droplets and smoke generated during the combustion process will accelerate and spread the flame, threatening people's lives and causing severe damage to buildings (Qiu, Li, Li & Zhang, 2018). This issue is particularly concerning in densely populated areas with high-rise buildings like Hong Kong. To address this, researchers are seeking inorganic materials to replace organic polymers in the production of reliable, sustainable, and high-performance SDRC coatings (Zhao, Hu, Ao, Xuan & Pei, 2020).

Geopolymer, a chemically-activated inorganic cement, may possess excellent thermal stability with low shrinkage, which could stay stable at up to 1000–1200 degrees Celsius while forming a more compacted ceramic structure (Wu et al., 2019). Geopolymer coatings are widely used as an environmentally friendly technology for construction and infrastructure applications (Jiang, Wang, Bao, Ni & Ling, 2020; Tatlisu, Aciksari, Celebi & Turan, 2022; Yuan et al., 2022; Zhao et al., 2021). As a new type of building material, geopolymer coatings improve both the greenness and durability of the material, which can reduce long-term costs by extending service life while reducing environmental impact (Omer & Noguchi, 2020; Sakulich, 2011; Sattary & Thorpe, 2016). The thermal insulation property of geopolymers is strongly related to their chemical composition as well as the presence of voids in the microstructure. There are many nano-scale air pores existing in the formed poly(sialate) framework, such nanopores can effectively reduce the thermal conductivity of geopolymers, thereby enhancing the thermal insulation ability (Yu et al., 2021). Besides, the nanopores provide numerous air-framework interfaces that could help to boost solar reflection through multiple Mie scattering, which is favorable for the daytime radiative cooling.

Phosphate activated geopolymer (PAGP) is a type of inorganic aluminosilicate polymer with a three-dimensional network structure of Si-O-Al-O-P units, consisting of silicon-oxygen tetrahedra, aluminum-oxygen tetrahedra and phosphorus-oxygen tetrahedral (Wan, Zhang & Zhang, 2022; Zribi & Baklouti, 2021). Compared to common alkali-activated geopolymers, phosphate activated geopolymers can achieve a higher strength and better thermal stability at high temperatures due to the partial replacement of Si-O bonds by P-O bonds in the frame structure (Louati, Hajjaji, Baklouti & Samet, 2014). Meanwhile, the intrinsic physico-chemical properties related to optical performance and cooling effect of PAGP are better compared to the alkali activated geopolymers. For example, the alkali metal ions in the structure of alkali activated geopolymers are electrically neutral with aluminum-oxygen tetrahedra by ionic bonding. Whereas in phosphate activated geopolymer, the system of [AlO_4], [SiO_4] and [PO_4] tetrahedra is electrically neutral with a balance of negative monovalent aluminum-oxygen tetrahedra and positive monovalent phosphorus-oxygen tetrahedra. The whole system is mainly covalently bonded and is therefore less affected by ionic polarization and relaxation polarization, which results in a relatively low dielectric constant and dielectric loss (Mo, Zhu, Cui, He & Gong, 2014).

The above analysis indicates that: (1) to achieve the large-scale application of the SDRC coatings, the aging problem and the weak high temperature resistance of the current polymer-based coatings still remain the major challenges; (2) PAGP shows great potential as the matrix for the SDRC coating to enhance its reliability and sustainability, while the functional fillers are the key to confirm both the good radiative cooling performance and the high temperature resistance of the PAGP-based coatings. Therefore, in this study, an environmentally friendly PAGP-based SDRC coating was developed under ambient conditions with microstructure modified by silica (SiO_2) and barium sulfate ($BaSO_4$) to reach a high infrared emissivity and a high solar reflectance as well as enhanced high-temperature resistance up to 1000 °C. The schematic illustration for the structure and cooling mechanism is shown in Fig. 1. The PAGP-based coating is expected to exhibit excellent high temperature resistance and maintain good cooling performance even after high temperature treatment. The outdoor filed tests were conducted on three identical model boxes under Hong Kong's climate from 30 April to 1 May 2023. The temperature reduction effect by the PAGP-based SDRC coating was compared with the surfaces of the commercial cooling coating and bare cement board. Results showed that the PAGP-based SDRC coating could achieve a sub-ambient cooling effect of 3.8 °C under direct solar radiation while the temperature of the commercial cooling coating coated board and the bare cement board was 5.2 °C and 27.7 °C higher than ambient temperature, respectively. The energy-saving performance of the PAGP-based SDRC coating applied on a typical small office was also analyzed across different climatic zones in China, which further highlighting the great energy-saving potential of the coating for large-scale application. This research provides a new approach for cost-effective and environmentally friendly coating techniques, which is expected to broaden the application scope of SDRC in the future.

2. Experimental and energy-saving assessment program

2.1. Raw materials

Metakaolin (MetaMax®, BASF) was used as a precursor with the XRF data shown in Table S1. $Al(H_2PO_4)_3$ solution (Hengyang Chemical) was used as the activator with the XRF data shown in Table S2. The Venator BLANC FIXE N-type nano-precipitated barium sulfate ($BaSO_4$, Macklin, 1 μm) and monodispersed silica nanosphere (nano-SiO_2, RHAWN, 30 ± 5 nm) were used to improve the reflectance and infrared emission of the coating.

2.2. Synthesis of the coatings

20 g $Al(H_2PO_4)_3$ solution was added to a beaker, followed by the metakaolin (MK) and about 25 g grinding beads for mixing and stirring. During the stirring process, 10–20 g of water were added according to the fluidity of the slurry. Then, SiO_2 and $BaSO_4$ were added in order. The detailed formulation proportion is shown in Table 1. The mixture was stirred at 800 rpm for 20 min, and then coated onto the substrate using a brush. The thickness of the above coating films after drying was 500 ± 50 μm, which was measured by a Micrometer thickness gauge. The hardness of the coating films was tested by Pushen Pencil hardness tester BY-500 g.

2.3. Optical measurements

Spectral reflectance of coating samples was measured using a PerkinElmer Lambda 1050+ UV/Visible/near-infrared broadband spectrometer equipped with an integrating sphere in accordance with ASTM E903–12 (Standard test method for Measuring solar absorption, reflectance, and transmittance of materials using an integrating sphere). The infrared emissivity of the coating samples was measured using a FTIR spectrometer with an integrating sphere (Vertex 70, Bruker).

2.4. Material characterizations

XRD analyses of metakaolin, $BaSO_4$, nano-SiO_2 and PAGP coatings with different fillers were carried out on a Bruker D8 ADVANCE A25X X-

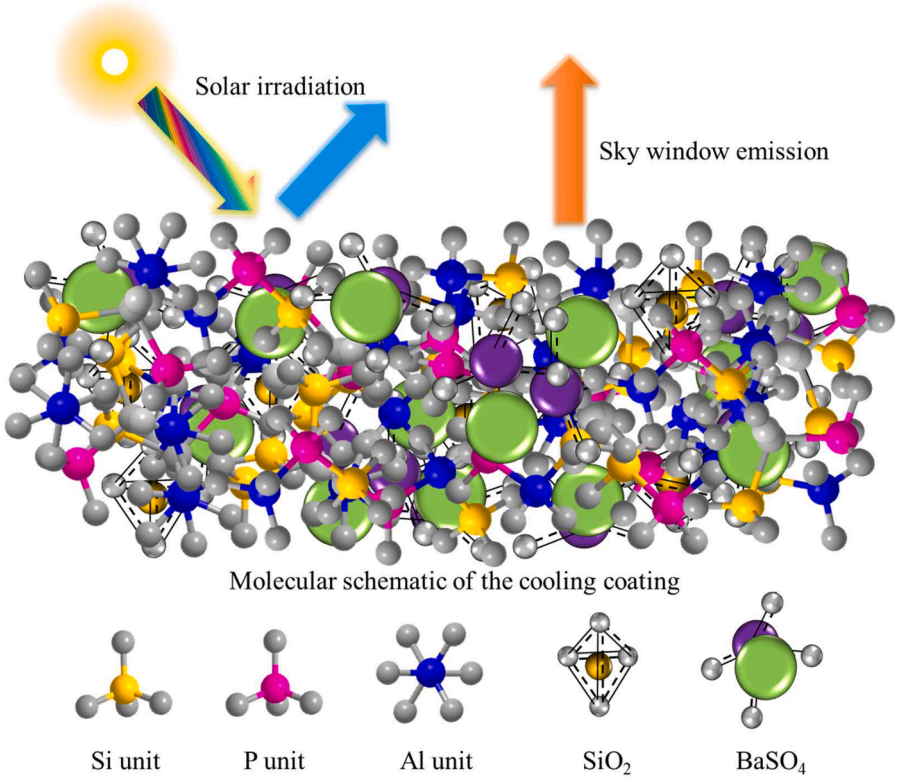

Fig. 1. Schematic diagram of molecular structure and optical mechanism of PAGP-based SDRC coating.

Table 1
The formulation proportion of PAGP cooling coating.

Component	$Al(H_2PO_4)_3$	Metakaolin	$BaSO_4$	SiO_2
mass%	17.5	12	70	0.5

ray diffractometer (Bruker AXS Ltd., Germany) to clarify the structural characteristics. FTIR spectra were tested on a Thermo Fisher Nicolet Is10 FT-IR spectrophotometer (Thermo Fisher, Germany) to analyze characteristic peaks of the above-mentioned materials. To determine the thermal stability and composition of coatings with different fillers, TGA was tested on the Rigaku Thermo Plus EVO2 thermogravimetric analyzer. SEM and EDS were conduct on TESCAN VEGA3 (TESCAN ORSAY HOLDING, Kohoutovice, Brno) to further determine the microstructure characteristics and element distribution of the PAGP-based SDRC coating. The BET analyses were conducted on Micromeritics ASAP 2460 Analyzer. The above characterization tests were performed only for the PAGP coating with optimum optical properties, which was determined by the optical test results.

2.5. Field tests

To evaluate its cooling performance, the PAGP-based SDRC coating with approximately a thickness of 500 microns was prepared on a standard cement board (according to GB/T 9271–2008) and then treated with a silane coupling agent KH-800. The MEMORY HiLOGGER LR8431–30 multi-channel temperature collector (Hioki, E.E. CORPORATION) was used to record the real-time temperature of different samples. K-type thermocouples were purchased from KAIPUSEN, KPD-TT-K-24-SLE-100 (Xinghua Suma Electric Appliance Co., LTD.). A combined mini weather-station (WS601-UMB, LUFFT) was used to measure and record solar irradiance, ambient, temperature, relative humidity, and wind speed.

2.6. Energy saving assessments

The whole building energy simulation software EnergyPlus was used to predict the energy saving performance of the PAGP-based SDRC coating under different climatic conditions as compared with the commercial cooling coating (a TiO_2 modified waterborne polymethyl methacrylate coating with solar reflectance of 85 %) and bare cement surface (GB/T 9271–2008). EnergyPlus is a widely-used simulation tool that can accurately model the energy consumption in buildings. The whole building simulation model was built in EnergyPlus. The simulation program and input parameters of the PAGP-based SDRC coating, commercial cooling coating and uncoated cement surface for the experiment boxes were first validated by experiment results, which was then extended to a typical small office building to analyze the annual energy saving performance of the PAGP-based SDRC coating in different climatic regions.

3. Results and discussion

3.1. Optical performance

PAGP coatings were modified with the addition of $BaSO_4$ and nano-SiO_2 to enhance the optical performance considering the following factors. First, nano-SiO_2 could effectively enhance the mechanical strength and durability through densifying the fine pore structure of PAGP composite, which is important for the coating application (Son, Liu, Chae & Lee, 2020; Wang, Dai, Ding & Xu, 2017; Zribi & Baklouti, 2021; Zribi, Samet & Baklouti, 2020). Meanwhile, nano-SiO_2 could play an important role in increasing the infrared emissivity due to the surface phonon polariton resonance at 9.7 μm (Baoping, Jinan, Hongjian, Yueming & Chunwei, 2005; Ravindra et al., 1994; Zhai et al., 2017). $BaSO_4$ with large optical bandgap was selected to further boost the solar reflectance as it has been proven to be an efficient way to increase the sunlight scattering (Li, Peoples, Yao & Ruan, 2021). Moreover, the $BaSO_4$ has good chemical inertness and high temperature resistance,

which is capable of further improving the stability and high temperature resistance of the PAGP-based SDRC coating (Chen, Zhou, Xu & Meng, 2013; Sifontes et al., 2015). As shown in Fig. 2a, the pure PAGP Matrix exhibited a moderate solar reflectance. After adding nano-SiO_2 into the PAGP, the reflectance of visible light increased significantly, but the high absorption of the UV and NIR radiation still remains the major problem. Adding $BaSO_4$ into the PAGP Matrix significantly increased the solar reflectance in all UV, Vis and NIR bands while the combination of nano-SiO_2 and $BaSO_4$ could reach an optimum result. The reflectance in the UV range decreased a little (from 0.7566 to 0.7443) when adding nano-SiO_2 into $BaSO_4$ modified PAGP coating, while the NIR reflectance increased and the overall reflectance became better (i.e., the overall solar reflectance increased from 0.9384 to 0.9468). The detailed results in different wavelength ranges are concluded in Table S3.

Further research was conducted to investigate the effects of the contents of $BaSO_4$ and nano-SiO_2 on the solar reflectance of the PAGP-based SDRC coating. When evaluating the influence of $BaSO_4$ contents, the nano-SiO_2 was not added. Results in Fig. 2b show that increasing the $BaSO_4$ content increased the solar reflectance of the PAGP coating, which reached 0.9064 at the addition 65 % $BaSO_4$ and further increased to the peak value of 0.9683 when the $BaSO_4$ content was 85 % (detailed data are shown in Table S4). However, it should be noted that the hardness of the coating is also an important parameter for the coating application. Therefore, with the aid of pencil hardness test (according to the ISO15184:2020) (Imae, Oonishi, Isaak, Yamamoto & Harima, 2017), the hardness of the PAGP coatings with different addition of $BaSO_4$ and nano-SiO_2 were tested (as shown in Figure S1). By considering both solar reflectance (Fig. 2b) and hardness (Figure S1a), PAGP with 70 % $BaSO_4$ could achieve the optimum solar reflectance while retaining a reasonable hardness, which was also chosen for the next-step tests to analyze the effects of the nano-SiO_2 content. Fig. 2c shows that adding nano-SiO_2 has a minor effect on the solar reflectance of the PAGP coating and the optimal value reached 0.9471 with 0.5 wt % nano-SiO_2 and shows no obvious change with the content of nano-SiO_2 further increases. Meanwhile, the hardness of the PAGP coating with 70 % $BaSO_4$ also increases by adding 0.5 wt % nano-SiO_2, as shown in Fig. S1b.

Fig. 2d shows the thermal IR emissivity of the optimized PAGP-based SDRC coating (i.e., 70 % $BaSO_4$ and 0.5 % SiO_2) in the spectral range of 6–20 μm. The results show that the optimized PAGP coating presents the highest IR emissivity up to 0.9634 within the atmospheric window (8–13 μm), and the total emissivity (6–20 μm) is 0.9593. The essential chemistry characteristics of matrix and fillers exhibit high absorbance in the region above 6.5 μm (details are presented in Fig. 3b), which contributed to the high emissivity.

3.2. *Materials characterizations*

XRD tests were conducted with a 9 kW Cu-Kα radiation source (λ = 1.5406 Å) and a scanning step of 0.02°. As shown in Fig. 3a, the characteristic peaks of the metakaolin include a broad dispersed peak that appears between 18° and 28° and a small sharp peak that appears at 25.5°, which indicated a mixed structure of semi-crystalline. A lower extent of crystallinity leads to a stronger reactivity which is suitable for

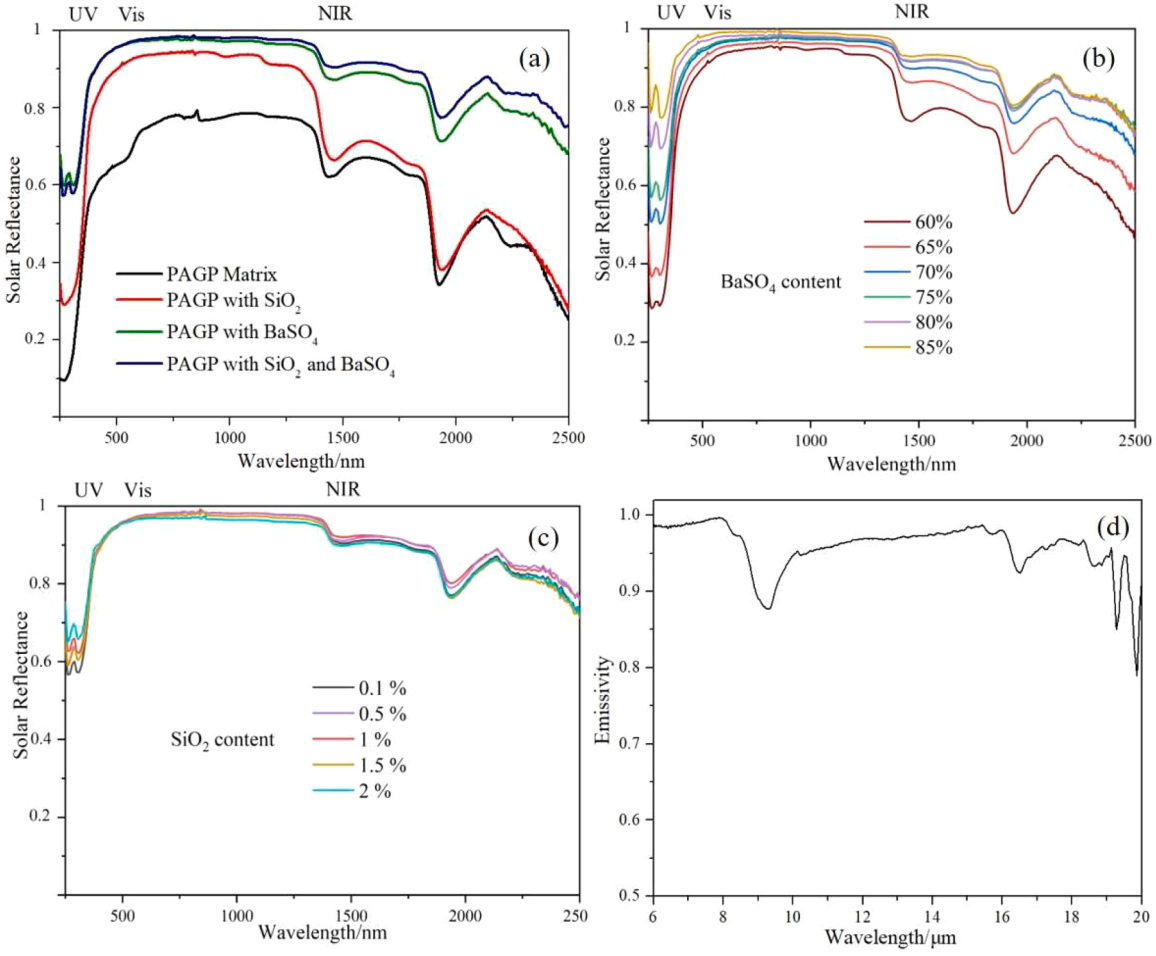

Fig. 2. Optical properties of coating samples with different functional fillers. (a) Solar reflectance of PAGP Matrix and PAGP coatings with different fillers. (b, c) Solar reflectance of PAGP coatings with varied addition ratios of $BaSO_4$ (b) and SiO_2 (c). (d) Infrared emissivity of the optimized PAGP-based SDRC coating.

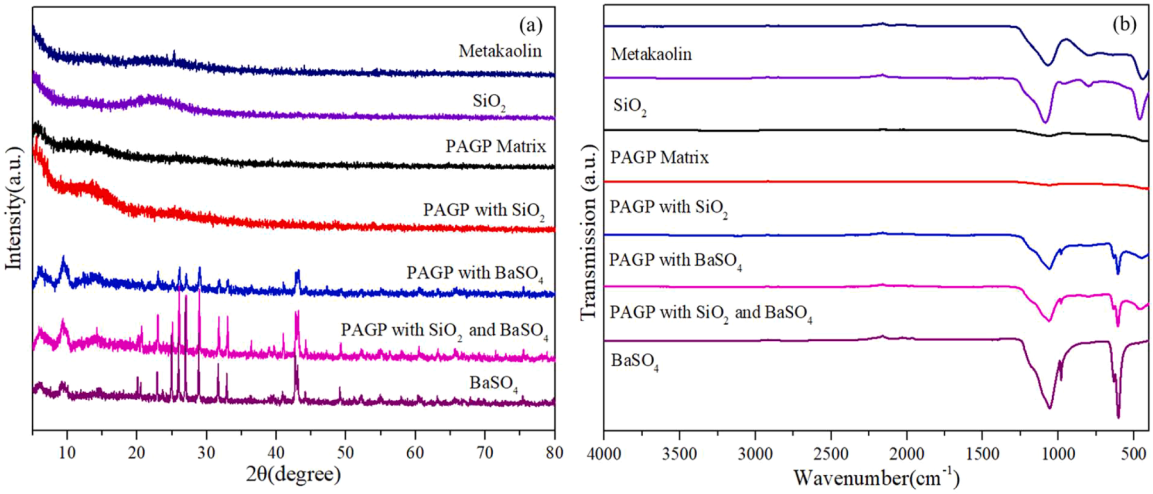

Fig. 3. XRD (a) and FTIR (b) of the raw materials, PAGP Matrix and PAGP coatings with different fillers.

geopolymerization reaction. Comparison of the XRD results of PAGP Matrix and PAGP with SiO_2 indicated that the small-amount addition of nano-SiO_2 changed the crystal structure and the grain diameter. According to the Bragg's Law, nano-SiO_2 changed the structure of PAGP Matrix to make a denser porous structure which was further characterized in the following BET test. As shown in Fig. 3a, the diffuse scattering range of the aluminosilicate is centered at 12°. From this it can be determined that an amorphous alumino-silico-phosphate (SiO_2·Al_2O_3·P_2O_5·nH_2O) was possibly formed (Katsiki, Hertel, Tysmans, Pontikes & Rahier, 2019; Wang et al., 2017). The samples with $BaSO_4$ all display the typical structure, which could refer to JCPDS No: 01–080–0512, including hkl values of $BaSO_4$ crystals (020), (101), (111), (200), (021), (210), (121), (211), (002), (140) and (212). The diffraction lines are sharp and intense, which could be related to the cube structure of crystals (Akyol & Cedimagar, 2016). The addition of $BaSO_4$ did not significantly change the crystal properties of the PAGP, so it can be inferred that the three-dimensional structure of PAGP covered and supported $BaSO_4$ particles.

FTIR transmission test was used to characterize the bulk properties of the samples, including functional groups and their bonding modes, as shown in Fig. 3b. Both PAGP Matrix and PAGP-based SDRC coating show the framework vibration modes of Si-O-Al, Si-O-P and/or Al-O-P bonds in the fingerprint region around 1020 cm^{-1}(Merabtene, Kacimi & Clastres, 2019), which contribute to high emissivity in the infrared region. Several widely dispersed weak bands appear in the FT-IR spectrum of the PAGP at around 1000 cm^{-1}, which led to the reduction of dielectric constant and thus could be beneficial for the enhancement of the infrared emissivity (Chen et al., 2020). The sulfur-oxygen stretching of inorganic sulfates are found in the region centered at 1055 cm^{-1}. The shoulder bands at 1177 cm^{-1} and 978 cm^{-1} are the symmetrical vibration of SO_4^{2-}(Ramaswamy, Vimalathithan & Ponnusamy, 2010). Because the addition content of $BaSO_4$ is more than half of the total content, most peaks of the PAGP-based SDRC coating are the characteristic peaks of $BaSO_4$.

Fig. 4 shows the micromorphology of the raw material, PAGP Matrix

Table 2
Median pore size and pore volume of PAGP Matrix and PAGP coatings with different fillers.

	PAGP Matrix	PAGP with SiO_2	PAGP with $BaSO_4$	PAGP with SiO_2 and $BaSO_4$
Median Pore Size (nm)	30.0	21.6	38.6	34.0
Pore Volume (cm^3/g)	0.002796	0.000524	0.007139	0.006565

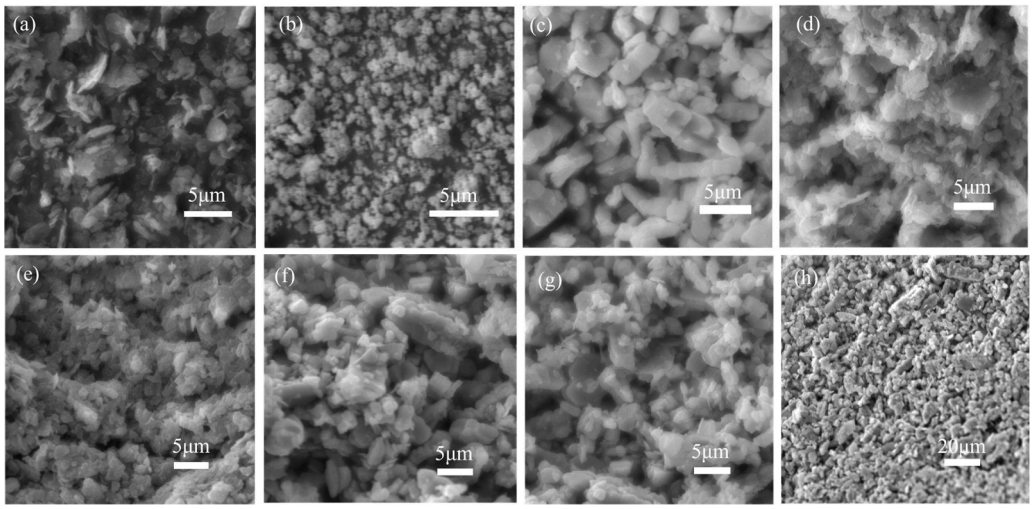

Fig. 4. microscopic morphology of metakaolin (a), SiO_2 (b), $BaSO_4$ (c), PAGP Matrix (d), PAGP with SiO_2 (e), PAGP with $BaSO_4$ (f), PAGP with SiO_2 and $BaSO_4$ (g), under 10,000× magnification, and PAGP with SiO_2 and $BaSO_4$ under 2000× magnification (h).

and PAGP coatings with different fillers, and the BET results of PAGP Matrix and PAGP coatings with different fillers are presented in Table 2. Metakaolin and $BaSO_4$ have sheet structures (Fig. 4a and c), while nano-SiO_2 is spherical (Fig. 4b). According to Mie scattering, if the radius of the fillers and the size of the micro/nano bulges and pores are comparable to the wavelength of the incident light, the incident light will be significantly scattered and be reflected back. The dielectric contrast near the geopolymer-$BaSO_4$, geopolymer-air and air-$BaSO_4$ interfaces can also efficiently enhance the solar reflectance. As it can be seen in Fig. 4c, PAGP Matrix endows microscale bulges and pores, which is inefficient for light scattering. As shown in Fig. 4d and e and Table 2, the addition of SiO_2 significantly decrease the pore volume of the PAGP Matrix from 0.002796 (PAGP Matrix) to 0.000524 (PAGP with SiO_2), and the median pore size decreases from 29.9 nm to 21.6 nm, which indicates that after adding nano-silica, the coating forms smaller and denser structures in the geo-polymerization reaction process (PAGP with SiO_2). However, the addition of the $BaSO_4$ increases both pore volume and median size of the PAGP matrix, but adding nano-SiO_2 in the small amount also changed the structure of the coating by decreasing the pore volume from 0.007139 to 0.006565, which reveals that nano-SiO_2 can better cover the $BaSO_4$ and form a dense porous structure (Fig. 4g and h, Fig. S2). The above results indicate that the addition of the SiO_2 in the PAGP based $BaSO_4$ coatings is able to form the smaller and denser pore structures, which is capable of increasing the solar reflectance (Fig. 2) and hardness (Figure S1) of the PAGP based SDRC coatings.

3.3. High temperature exposure

The thermal stability of the PAGP-based coatings was tested through TGA to provide the information on the mass change of the sample over the temperature rise, which was caused by thermal decomposition and phase transitions. The argon atmosphere was applied as the protective gas for the entire range of elevated temperatures from 30 to 1000 °C. As shown in Fig. 5a and b, the graphs of PAGP Matrix and PAGP with SiO_2 are typical three-stage exothermic curve of the geopolymer composite (Wang et al., 2017). For the PAGP Matrix, a mass loss of approximately 10 % occurred with a sharp endothermic peak between 110 °C and 142 °C due to dehydration. Another endothermic peak appeared at about 183 °C, with a continued mass loss of around 2 %, which was attributed to the decomposition of $AlH_3(PO_4)_2 \cdot 3H_2O$. From 230 °C to 1000 °C, the mass almost remained unchanged with a recorded mass loss of 0.9 % because of the dihydroxylation of hydroxyl groups. For the PAGP with SiO_2, a mass loss of approximately 15 % occurred with a sharp endothermic peak between 119 °C and 192 °C due to dehydration. Another endothermic peak appeared at about 183 °C, with a continued mass loss of around 2.5 %, which was attributed to the decomposition of $AlH_3(PO_4)_2 \cdot 3H_2O$. From 231 °C to 1000 °C, the mass almost remained unchanged. About 2 % mass loss was recorded because of the dihydroxylation of hydroxyl groups. For both PAGP with $BaSO_4$ and PAGP with SiO_2 and $BaSO_4$, about 2.2 % of mass loss were obtained between 135 °C and 186 °C, and 6.5 % of mass loss were recorded at 1000 °C. It's clearly that the addition of $BaSO_4$ improved the high-temperature stability of both pure PAGP and nano-SiO_2 modified PAGP coating under elevated temperatures, which demonstrated great high-temperature resistance of the nano-SiO_2 and $BaSO_4$ modified PAGP coating.

As shown in the Fig. 6, XRD tests were conducted on samples after high temperature treatments. The treatments started at room temperature with a heating rate of 30 °C min^{-1} and lasted for 1 h. Compared to XRD results at room temperature (Fig. 3a), the 100 °C exposed sample presented similar peaks, indicating that the PAGP remain gel structure under 100 °C. While after the 200 °C and 800 °C exposure, when the dehydration and phase change occurred, PAGP Matrix and PAGP with SiO_2 presented the peaks of nepheline and quartz (Cheng-Yong, Yun-Ming, Abdullah & Hussin, 2017), which are in accordance with the

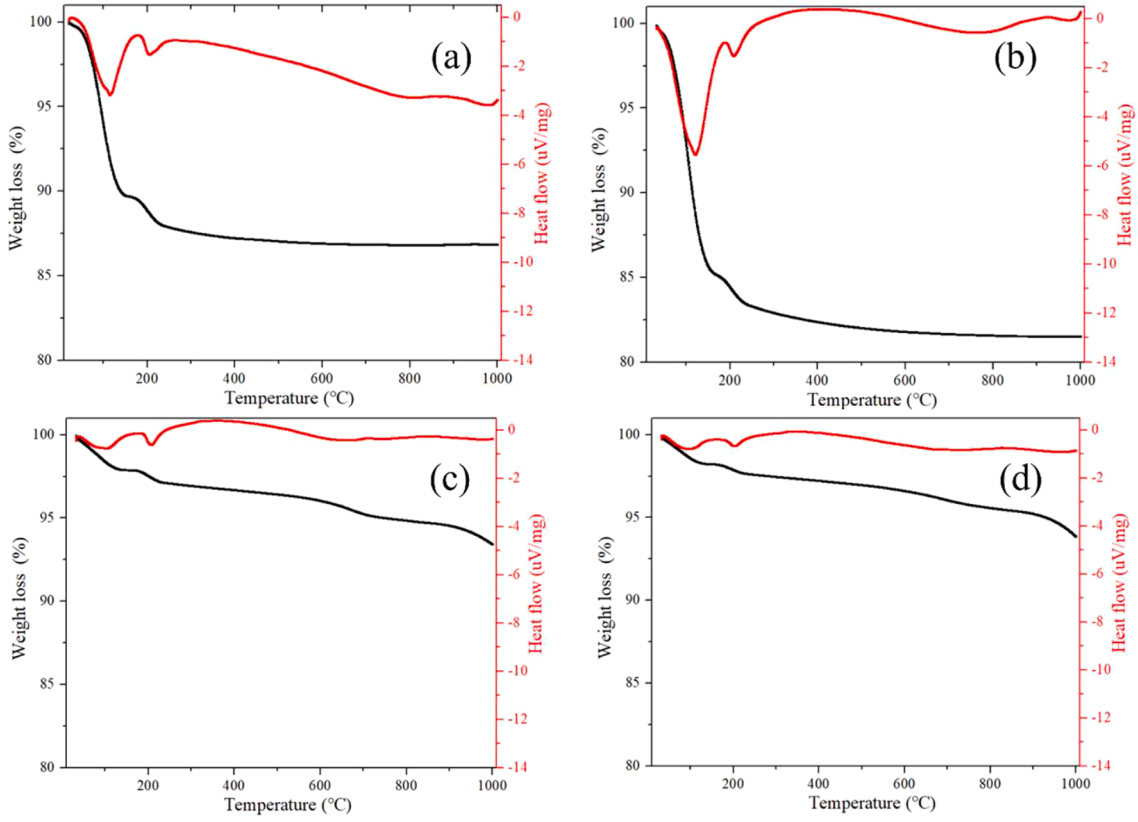

Fig. 5. TGA-DTA thermograms of PAGP Matrix (a), PAGP with SiO_2 (b), PAGP with $BaSO_4$ (c), and PAGP with SiO_2 and $BaSO_4$ (d), subjected to elevated temperatures (from 30 to 1000 °C).

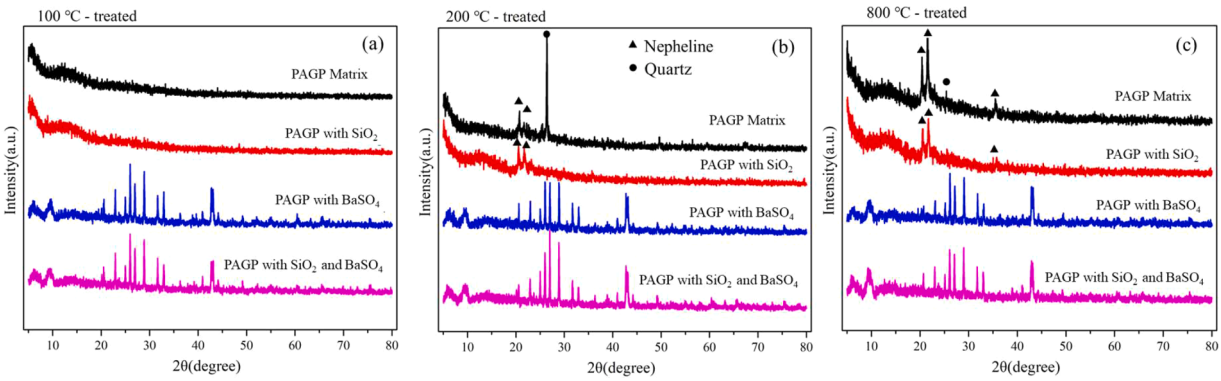

Fig. 6. XRD of PAGP Matrix and PAGP coatings with different fillers after high temperature exposure.

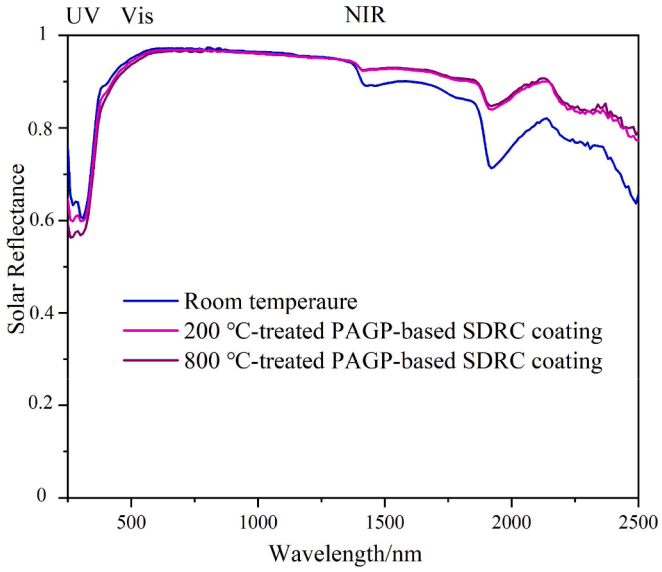

Fig. 7. Solar reflectance of PAGP-based SDRC coating after high temperature exposure.

weight loss curve of the TGA results. For the comparison of XRD results of PAGP Matrix and PAGP with $BaSO_4$ after high temperature treatments, little change had been observed which means that $BaSO_4$ possess good high temperature resistance.

More importantly, the excellent thermal stability of the PAGP-based SDRC coating provide a potential for them to be applied at high temperatures conditions. As shown in Fig. 7, little change of solar reflectance was observed for the PAGP-based SDRC coating after 200 °C and 800 °C exposures. To be specific, after 200 °C exposure, the solar reflectance changed from 0.9333 to 0.9330, and to 0.9290 after 800 °C exposure (refer to Table 3), which indicated that the PAGP-based SDRC coating could retain optimum solar reflectance after high-temperature exposure.

Table 3
Solar reflectance of PAGP coating after high temperature exposure.

PAGP-based SDRC coating	UV	Vis	NIR	Total
At room temperature	0.7674	0.9422	0.9373	0.9333
After 200 °C exposure	0.7437	0.9343	0.9463	0.9330
After 800 °C exposure	0.7200	0.9271	0.9468	0.9290

From the above analysis, it can be concluded that by incorporating the nano-SiO_2 and $BaSO_4$, both optical performance and high-temperature resistance of the PAGP-based SDRC coating can be improved significantly, which is capable of achieving a high infrared emissivity of 0.9634 and a solar reflectance of 0.9471 and retaining thermal and optical stability up to 1000 °C. The material characterization results indicated that $BaSO_4$ is the major contributor to enhance the optical performance and high-temperature resistance of the PAGP-based SDRC coating while the addition of the nano-SiO_2 in the small amount can further increase its solar reflectance by adjusting the pore structure of the coating.

3.4. Field tests

As shown in Fig. 8, the installation of the experimental test rig (samples with experiment boxes, temperature data logger, and a weather station) was set up on a rooftop and exposed to direct sunlight in Hong Kong on April 30 to 1 May 2023 (Xue et al., 2020; Yang, Fu, Xue, Lei & Dai, 2023). The relative humidity was stable at 74.29 % and the average wind speed was 0.5376 m/s. The recorded temperature curves are shown in Fig. 8. The temperature of the PAGP-based SDRC coated board (T_{PAGP}) was constantly below the ambient temperature, and the temperate of uncoated board ($T_{uncoated}$) and the commercial cooling coating (T_{CCC}) was well above the ambient temperature by maximum values of 5.2 °C and 27.7 °C, respectively under the direct sunlight. The cooling effect of the PAGP-based SDRC coating could be up to 3.8 °C lower than the ambient temperature during daytime without any energy input. The average temperature for the 24 h and midday periods is shown in Table S7.

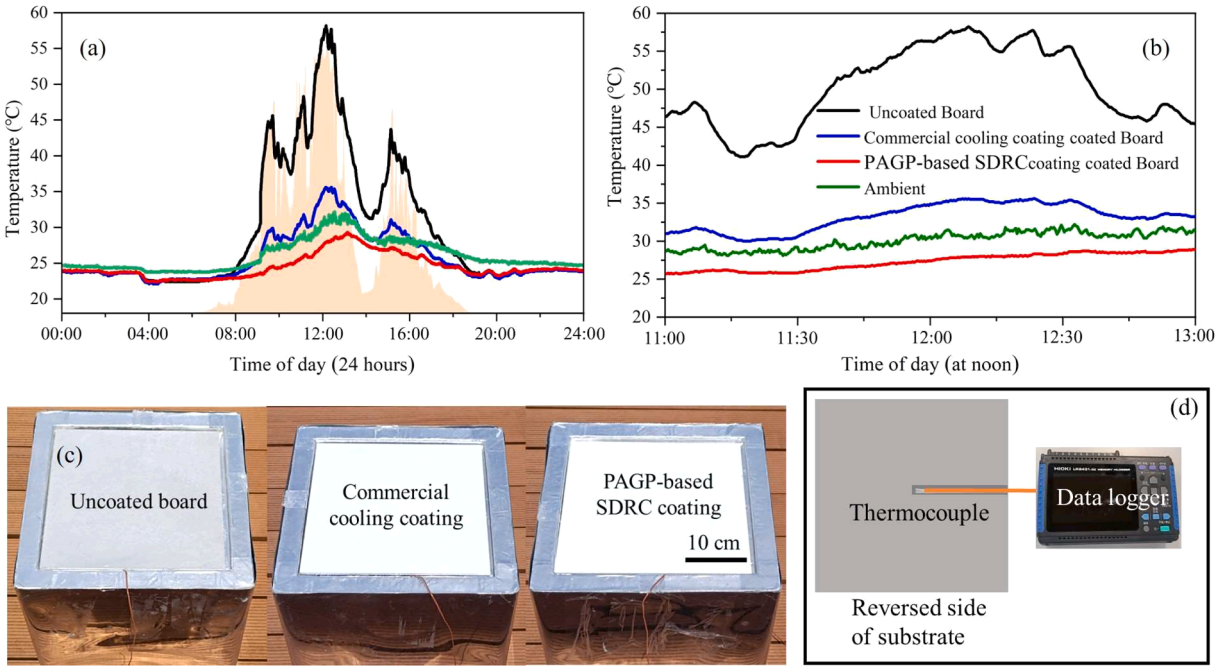

Fig. 8. Comparison of the PAGP-based SDRC coating coated board, commercial cooling coating coated board, and uncoated board. Graph of temperature change for 24 h with the global horizontal irradiance (a). Graph of temperature change in direct sunlight at noon (b). Digital photo of the field test chamber (c). Schematic diagram of the test device (d).

3.5. Energy saving analysis

In EnergyPlus, the radiative heating transfer property and solar absorption property of building components are calculated based on average spectra values, e.g., thermal absorptance (ε), solar absorptance (α), and visible absorptance (α_{vis}), which can be calculated as follows:

$$\alpha = \frac{\int_0^\infty a(\lambda,\theta) I_{solar}(\lambda) d\lambda}{\int_0^\infty I_{solar}(\lambda) d\lambda} \quad (1)$$

$$\alpha_{vis} = \frac{\int_{Visible} a(\lambda,\theta) I_{solar}(\lambda) d\lambda}{\int_0^\infty I_{solar}(\lambda) d\lambda} \quad (2)$$

$$\varepsilon = \frac{\int_0^\infty \varepsilon(\lambda) I_{bb}(\lambda,T) d\lambda}{\int_0^\infty I_{bb}(\lambda,T) d\lambda} \quad (3)$$

Where $\alpha(\lambda, \theta)$is spectral directional absorptivity of the envelope surface;$\varepsilon(\lambda)$ is hemisphere spectral emissivity of the envelope surface; I_{solar} is the spectra solar irradiance; $I_{bb}(\lambda, T)$ is the spectral radiation intensity of a blackbody at temperature T.

The experiment boxes used in the test program reported in the previous sessions were first modeled to validate the input settings of the PAGP-based SDRC coating, commercial cooling coating and uncoated cement surface in EnergyPlus. The input parameters of the experiment boxes with different coatings including the dimensions, box configurations Table 4), optical characteristics of different coatings (calculated from the measured optical properties via Eqs. (1)–(3), and the weather data (e.g., solar irradiance, wind speed, relative humidity, and ambient temperature) are all set to be the same as in the field tests. As shown in Fig. 9, the simulated temperatures of the standard cement boards applied with different coatings are compared with the measured results. In general, the predicted temperatures agree well with the tested results (Fig. 9a). Furthermore, as shown in Fig. 9b, the deviations between the simulation and tested results for PAGP-based SDRC coating, commercial

Table 4
Thermal property of the experiment box.

Envelope	Construction (from outside to inside)	Thickness, m	Conductivity, W/m·k	Density, kg/m^3	Specific heat, J/kg·k
Wall	VIP board	0.048	0.002	300	900
Floor	VIP board	0.048	0.002	300	900
Roof	Cement board	0.004	1.6	3000	850

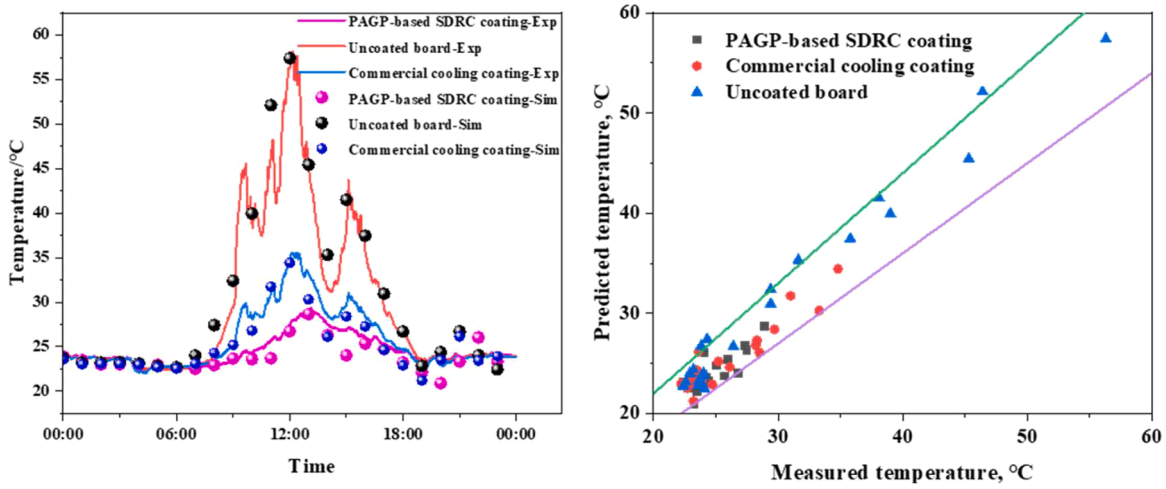

Fig. 9. Validation of the simulation program.

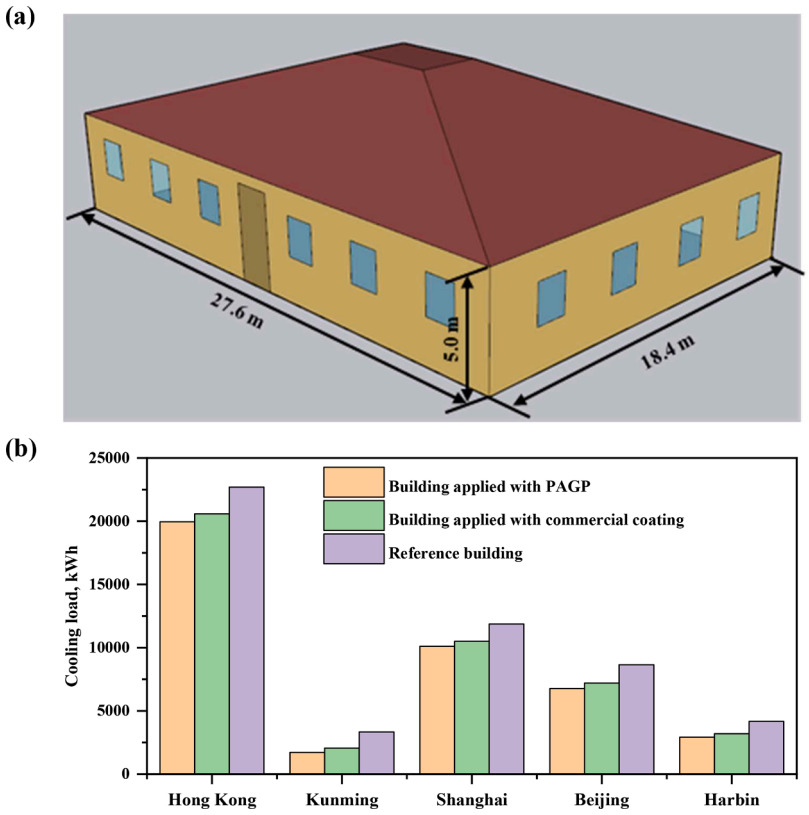

Fig. 10. (a) Schematic diagram of the modeled simple office building; (b) Annual cooling loads of the simple office building in indifferent climatic regions.

cooling coating, and uncoated cement surface all fall within ±10 %, indicating the accuracy of the input parameters and settings for the modeled experiment boxes applied with different coatings (Xuan et al., 2022).

Then, the simulation program was extended to the whole building simulation with the validated input parameters for the PAGP-based SDRC coating, commercial cooling coating and uncoated cement surface. As shown in Fig. 10a. The reference building to be modeled is a single-story office building according to ANSI/ASHRAE/IES Standard 90.1 (Office of Energy Efficiency & Renewable Energy, 2000), whose length, width, and height are 27.6 m, 18.4 m, and 5.0 m respectively. The building envelope information and its thermophysical properties are presented in Table 5 and the model definitions are listed in Table 6. The PAGP-based SDRC coating and commercial cooling coating were

Table 5
Envelop structures and thermophysical properties of the modeled simple office buildings.

	Materials (from outside to inside)	Thickness (m)	Thermal Conductivity (W/m·K)	Density (kg/m^3)	Specific heat (J/kg·K)
Exterior Walls	Heavy-weight Concrete	0.2033	1.7296	2243	837
	Wall insulation	0.0452	0.0432	91	837
	Gypsum	0.0127	0.16	784.9	830
Floor	Heavy weight Concrete	0.1016	1.311	2240	836.8
	No-mass Carpet pad	–	0.1	–	–
Door	F08 Metal Surface	0.0008	45.28	7824	500
	Insulation board	0.0254	0.03	43	1210
Roof	Roof Membrane	0.0095	0.16	1121.29	1460
	Roof insulation	0.2105	0.049	265	836.8
	Metal decking	0.0015	45.006	7680	418.4
Window	Clear glass	0.003	0.0415	–	–

Table 6
Model definitions.

Items	Values
Running period	9:00 – 18:00, 1st Jan to 31st Dec
A/C system	Ideal air load system
Cooling setpoint	24 °C
Electric Lighting	10.66 W/m^2
Electric load	6.89 W/m^2
Infiltration	0.0003026 m/s/floor area(m^2)

implemented to the surface of the building model including both the roof and walls. The optical characteristics of the standard bare cement board (Fig. S3) was also applied to the building surface as the reference case. Other model definitions are also summarized in Table 5. An ideal air load system is equipped for the office building and the cooling setpoint temperature is 24 °C.

To investigate the energy-saving performance of the PAGP-based SDRC coating under different climatic regions, five typical cities across China that represent different climate characteristics were chosen, i.e., Hong Kong (hot summer and warm winter), Kunming (temperate), Shanghai (hot summer and cold winter), Beijing (cold winter), and Harbin (severely cold winter). As shown in Fig. 10, the cooling effect of the PAGP-based SDRC coating is significant in all five cities especially in the hot climatic city, i.e., Hong Kong, due to the longer cooling duration. In Hong Kong, a typical cooling-dominated city, the cooling load of the reference building is the highest among five cities that reaches 22,694.78 kWh. After applying the PAGP-based SDRC coating, the cooling load can be reduced by 2742.51 kWh. In other climatic cities with higher latitudes, i.e., in Kunming, Shanghai, Beijing, and Harbin, the need for the space cooling reduces, but the cooling effect by the PAGP-based SDRC coating is still remarkable. In these four cites, PAGP-based SDRC coating saves the building cooling load by 1623.82 kWh, 1760.71 kWh, 1881.62 kWh, and 1240.87 kWh, respectively. Compared with the commercial cooling coating, the PAGP-based SDRC coating also yields a higher energy-saving performance across all selected climatic cities in China, with the total cooling load saving ranges between 266.61 kWh to 627.75 kWh, which further demonstrates the excellent energy saving potential of the PAGP-based SDRC coating in building applications.

4. Conclusions

In summary, to solve the aging problem and weak high-temperature resistance of the commonly used organic polymer-based SDRC coatings, a phosphate activated geopolymer-based (PAGP) inorganic coating was proposed and modified with nano-SiO_2 and $BaSO_4$ to achieve desired optical performance and high-temperature resistance. Based on a comprehensive experimental program, the following conclusions have been arrived:

(1) The optimized PAGP coating could achieve a high solar reflectance of 0.9471 and high infrared emissivity of 0.9634, as well as a sub-ambient cooling effect of 3.8 °C below the ambient temperature under the direct sunlight in Hong Kong.
(2) It was confirmed that the developed the PAGP-based SDRC coating has excellent high temperature resistance and could maintain well its performance after high temperature exposure (e.g., even at 1000 °C).
(3) A simulation model of the typical simple office building was built in EnergyPlus and validated through comparing with experimental results. The model was further extended to five different climatic cities across China, i.e., Hong Kong, Kunming, Shanghai, Beijing, and Harbin. It is indicated that the PAGP-based SDRC coating could save 1240.87∼2742.51 kWh per year of cooling load compared with the uncoated cement surface and could save 266.61∼627.75 kWh per year of cooling load compared with the commercial cooling coating.

This PAGP-based SDRC coating has good potential for applications in infrastructures with a cooling need under direct sunlight even under a high service temperature condition, which could help to broaden the applicability and provide a cost-effective and environmentally friendly passive cooling solution.

Declaration of Competing Interest

The authors declare that they have no known competing financial interests or personal relationships that could have appeared to influence the work reported in this paper.

Data availability

Data will be made available on request.

Acknowledgements

We acknowledge the financial support by RGC General Research Fund (Project No. 15223120), RGC Collaborative Research Fund (Project No. C5051–22GF), Research Institute for Sustainable Urban Development (Project No. 1-BBWX) and Research Institute for Smart Energy (Project No. CDBL) of The Hong Kong Polytechnic University. The first author would like to thank the PhD studentship provided by the Hong Kong Polytechnic University.

Supplementary materials

Supplementary material associated with this article can be found, in the online version, at doi:10.1016/j.scs.2023.104992.

References

Akyol, E., & Cedimagar, M. (2016). Size and morphology controlled synthesis of barium sulfate: Size and morphology controlled synthesis of barium sulfate. *Crystal Research and Technology, 51*, 393–399. https://doi.org/10.1002/crat.201600046

Baoping, L., Jinan, T., Hongjian, L., Yueming, S., & Chunwei, Y. (2005). Structure and infrared emissivity of polyimide/mesoporous silica composite films. *Journal of Solid State Chemistry, 178*(3), 650–654. https://doi.org/10.1016/j.jssc.2004.12.010

Chen, G., Wang, Y., Qiu, J., Cao, J., Zou, Y., Wang, S., & Zhou, Y. (2020). Robust inorganic daytime radiative cooling coating based on a phosphate geopolymer. *Acs Applied Materials & Interfaces, 12*(49), 54963–54971. https://doi.org/10.1021/acsami.0c15799

Chen, R., Zhou, J., Xu, B., & Meng, X. (2013). Preparation of TiO2–$BaSO_4$ composite microparticles and their photocatalytic activity. *Chemical Engineering Journal, 218*, 24–31. https://doi.org/10.1016/j.cej.2012.12.039

Cheng-Yong, H., Yun-Ming, L., Abdullah, M. M. A. B., & Hussin, K. (2017). Thermal resistance variations of fly ash geopolymers: foaming responses. *Scientific Reports, 7*(1), 45355. https://doi.org/10.1038/srep45355

Hu, M., Zhao, B., Suhendri, Cao, J., Wang, Q., Riffat, S., & Pei, G. (2021). Feasibility of realizing daytime solar heating and radiative cooling simultaneously with a novel structure. *Sustainable Cities and Society, 74*, Article 103224. https://doi.org/10.1016/j.scs.2021.103224

Imae, I., Oonishi, T., Isaak, I. S., Yamamoto, S., & Harima, Y. (2017). Facile fabrication of transparent conductive graphene/silica composite films with high mechanical strength. *Synthetic Metals, 224*, 33–35. https://doi.org/10.1016/j.synthmet.2016.12.020

Jiang, C., Wang, A., Bao, X., Ni, T., & Ling, J. (2020). A review on geopolymer in potential coating application: Materials, preparation and basic properties. *Journal of Building Engineering, 32*, Article 101734. https://doi.org/10.1016/j.jobe.2020.101734

Katsiki, A., Hertel, T., Tysmans, T., Pontikes, Y., & Rahier, H. (2019). Metakaolinite phosphate cementitious matrix: Inorganic polymer obtained by acidic activation. *Materials, 12*(3), 442.

Li, X., Peoples, J., Yao, P., & Ruan, X. (2021). Ultrawhite $BaSO_4$ paints and films for remarkable daytime subambient radiative cooling. *Acs Applied Materials & Interfaces, 13*(18), 21733–21739. https://doi.org/10.1021/acsami.1c02368

Liu, M., Li, X., Li, L., Li, L., Zhao, S., Lu, K., & Zou, C. (2023). Continuous photothermal and radiative cooling energy harvesting by VO_2 smart coatings with switchable broadband infrared emission. *ACS Nano, 17*(10), 9501–9509. https://doi.org/10.1021/acsnano.3c01755

Louati, S., Hajjaji, W., Baklouti, S., & Samet, B. (2014). Structure and properties of new eco-material obtained by phosphoric acid attack of natural Tunisian clay. *Applied Clay Science, 101*, 60–67. https://doi.org/10.1016/j.clay.2014.07.015

Mandal, J., Fu, Y., Overvig, A. C., Jia, M., Sun, K., Shi, N. N., & Yang, Y. (2018). Hierarchically porous polymer coatings for highly efficient passive daytime radiative cooling. *Science, 362*(6412), 315–319. https://doi.org/10.1126/science.aat9513

Merabtene, M., Kacimi, L., & Clastres, P. (2019). Elaboration of geopolymer binders from poor kaolin and dam sludge waste. *Heliyon, 5*, e01938. https://doi.org/10.1016/j.heliyon.2019.e01938

Mo, B.-H., Zhu, H., Cui, X.-M., He, Y., & Gong, S.-Y. (2014). Effect of curing temperature on geopolymerization of metakaolin-based geopolymers. *Applied Clay Science, 99*, 144–148. https://doi.org/10.1016/j.clay.2014.06.024

Office of Energy Efficiency & Renewable Energy. 2000 Homepage. Retrieved from https://www.energycodes.gov/prototype-building-models.

Omer, A. M. (2008). Energy, environment and sustainable development. *Renewable and Sustainable Energy Reviews, 12*(9), 2265–2300. https://doi.org/10.1016/j.rser.2007.05.001

Omer, M. A. B., & Noguchi, T. (2020). A conceptual framework for understanding the contribution of building materials in the achievement of Sustainable Development Goals (SDGs). *Sustainable Cities and Society, 52*, Article 101869. https://doi.org/10.1016/j.scs.2019.101869

Pan, Y., & Zhang, L. (2020). Data-driven estimation of building energy consumption with multi-source heterogeneous data. *Applied Energy, 268*, Article 114965. https://doi.org/10.1016/j.apenergy.2020.114965

Qiu, X., Li, Z., Li, X., & Zhang, Z. (2018). Flame retardant coatings prepared using layer by layer assembly: A review. *Chemical Engineering Journal, 334*, 108–122. https://doi.org/10.1016/j.cej.2017.09.194

Raman, A. P., Anoma, M. A., Zhu, L., Rephaeli, E., & Fan, S. (2014). Passive radiative cooling below ambient air temperature under direct sunlight. *Nature, 515*(7528), 540–544. https://doi.org/10.1038/nature13883

Ramaswamy, V., Vimalathithan, R. M., & Ponnusamy, V. (2010). Synthesis and characterization of $BaSO_4$ nano-particles using micro-emulsion technique. *Advances in Applied Science Research*, 1.

Ravindra, N., Tong, F., Kosonocky, W., Markham, J., Liu, S., & Kinsella, K. (1994). Temperature dependent emissivity measurements of Si, SiO_2/Si, and HgCdTe. In *MRS Online Proceedings Library (OPL)* (p. 342).

Rong, X., Wang, Z., Xing, X., & Zhao, L. (2021). Review on the adhesion of geopolymer coatings. *ACS Omega, 6*(8), 5108–5112. https://doi.org/10.1021/acsomega.0c06343

Sakulich, A. R. (2011). Reinforced geopolymer composites for enhanced material greenness and durability. *Sustainable Cities and Society, 1*(4), 195–210. https://doi.org/10.1016/j.scs.2011.07.009

Sattary, S., & Thorpe, D. (2016). Potential carbon emission reductions in australian construction systems through bioclimatic principles. *Sustainable Cities and Society, 23*, 105–113. https://doi.org/10.1016/j.scs.2016.03.006

Sheng, S.-Z., Wang, J.-L., Zhao, B., He, Z., Feng, X.-F., Shang, Q.-G., & Yu, S.-H. (2023). Nanowire-based smart windows combining electro- and thermochromics for dynamic regulation of solar radiation. *Nature Communications, 14*(1), 3231. https://doi.org/10.1038/s41467-023-38353-4

Sifontes, Á.B., Cañizales, E., Toro-Mendoza, J., Ávila, E., Hernández, P., Delgado, B.A., . . . Cruz-Barrios, E.J.J.O. N. (2015). Obtaining highly crystalline barium sulphate nanoparticles via chemical precipitation and quenching in absence of polymer stabilizers. 2015, 6–6.

Son, S., Liu, Y., Chae, D., & Lee, H. (2020). Cross-linked porous polymeric coating without a metal-reflective layer for sub-ambient radiative cooling. *Acs Applied Materials & Interfaces, 12*(52), 57832–57839.

Song, J., Zhang, W., Sun, Z., Pan, M., Tian, F., Li, X., & Deng, X. (2022). Durable radiative cooling against environmental aging. *Nature Communications, 13*(1), 4805. https://doi.org/10.1038/s41467-022-32409-7

Sun, J., Wang, J., Guo, T., Bao, H., & Bai, S. (2022). Daytime passive radiative cooling materials based on disordered media: A review. *Solar Energy Materials and Solar Cells, 236*, Article 111492. https://doi.org/10.1016/j.solmat.2021.111492

Tatlisu, G. C., Aciksari, C., Celebi, S., & Turan, S. (2022). Developing a hollow glass microsphere/geopolymer thermal insulation composite for hot metal surface coating. *Ceramics International, 48*(9), 11924–11939. https://doi.org/10.1016/j.ceramint.2022.01.042

Wan, Q., Zhang, R., & Zhang, Y. (2022). Structure and properties of phosphate-based geopolymer synthesized with the spent fluid catalytic-cracking (SFCC) Catalyst. *Gels, 8*(2). https://doi.org/10.3390/gels8020130

Wang, Y.-S., Dai, J.-G., Ding, Z., & Xu, W.-T. (2017). Phosphate-based geopolymer: Formation mechanism and thermal stability. *Materials Letters, 190*, 209–212. https://doi.org/10.1016/j.matlet.2017.01.022

Wu, Y. G., Lu, B. W., Bai, T., Wang, H., Du, F. P., Zhang, Y. F., & Wang, W. J. (2019). Geopolymer, green alkali activated cementitious material: Synthesis, applications and challenges. *Construction and Building Materials, 224*, 930–949. https://doi.org/10.1016/j.conbuildmat.2019.07.112

Xuan, Q., Zhao, B., Wang, C., Li, L., Lu, K., Zhai, R., ... Management. (2022). Development, testing, and evaluation of the daylighting, thermal, and energy-saving performance of semitransparent radiative cooling glass in cooling-dominated regions. 273, 116443.

Xue, X., Qiu, M., Li, Y., Zhang, Q. M., Li, S., Yang, Z., & Fan, S. (2020). Creating an eco-friendly building coating with smart subambient radiative cooling. *Advanced Materials, 32*(42), Article 1906751. https://doi.org/10.1002/adma.201906751

Yang, N., Fu, Y., Xue, X., Lei, D., & Dai, J.-G. (2023). Geopolymer-based sub-ambient daytime radiative cooling coating. *EcoMat, 5*(2), e12284. https://doi.org/10.1002/eom2.12284

Younes, J., Ghali, K., & Ghaddar, N. (2022). Diurnal selective radiative cooling impact in mitigating urban heat island effect. *Sustainable Cities and Society, 83*, Article 103932. https://doi.org/10.1016/j.scs.2022.103932

Yu, X., Chan, J., & Chen, C. (2021). Review of radiative cooling materials: Performance evaluation and design approaches. *Nano Energy, 88*, Article 106259. https://doi.org/10.1016/j.nanoen.2021.106259

Yuan, J., Yin, H., Yuan, D., Yang, Y., & Xu, S. (). On daytime radiative cooling using spectrally selective metamaterial based building envelopes. *Energy, 242*, Article 122779. https://doi.org/10.1016/j.energy.2021.122779

Zhai, Y., Ma, Y., David, S. N., Zhao, D., Lou, R., Tan, G., & Yin, X. (2017). Scalable-manufactured randomized glass-polymer hybrid metamaterial for daytime radiative cooling. *Science, 355*(6329), 1062–1066. https://doi.org/10.1126/science.aai7899

Zhao, B., Hu, M., Ao, X., Chen, N., & Pei, G. (2019). Radiative cooling: A review of fundamentals, materials, applications, and prospects. *Applied Energy, 236*, 489–513. https://doi.org/10.1016/j.apenergy.2018.12.018

Zhao, B., Hu, M., Ao, X., Xuan, Q., & Pei, G. (2020). Spectrally selective approaches for passive cooling of solar cells: A review. *Applied Energy, 262*, Article 114548. https://doi.org/10.1016/j.apenergy.2020.114548

Zhao, J., Tong, L., Li, B., Chen, T., Wang, C., Yang, G., & Zheng, Y. (2021). Eco-friendly geopolymer materials: A review of performance improvement, potential application and sustainability assessment. *Journal of Cleaner Production, 307*, Article 127085. https://doi.org/10.1016/j.jclepro.2021.127085

Zribi, M., & Baklouti, S. (2021). Phosphate-based geopolymers: A critical review. *Polymer Bulletin*. https://doi.org/10.1007/s00289-021-03829-0

Zribi, M., Samet, B., & Baklouti, S. (2020). Mechanical, microstructural and structural investigation of phosphate-based geopolymers with respect to P/Al molar ratio. *Journal of Solid State Chemistry, 281*, Article 121025. https://doi.org/10.1016/j.jssc.2019.121025